ACS APPLIED MATERIALS & INTERFACES

Research Article

www.acsami.org

# Highly Thermostable, Flexible, Transparent, and Conductive Films on Polyimide Substrate with an AZO/AgNW/AZO Structure

Qijin Huang,[†] Wenfeng Shen,*[,†] Xingzhong Fang,[†] Guofei Chen,[†] Ye Yang,[†] Jinhua Huang,[†] Ruiqin Tan,[‡] and Weijie Song*[,†]

[†] Ningbo Institute of Material Technology and Engineering, Chinese Academy of Sciences, Ningbo, Zhejiang 315201, China

[‡]Faculty of Information Science and Engineering, Ningbo University, Ningbo, Zhejiang 315211, China

**ABSTRACT:** Flexible transparent conductive films (TCFs) are used in a variety of optoelectronic devices. However, their use is limited due to poor thermostability. We report hybrid TCFs incorporation in both aluminum-doped zinc oxide (AZO) and silver nanowires (AgNWs). The layered AZO/AgNWs/AZO structure was deposited onto a transparent polyimide (PI) substrate and displayed excellent thermostability. When heated to 250 °C for 1 h, the change in resistivity ($R_c$) was less than 10% ($R_c$ of pure AgNW film > 500) while retaining good photoelectric properties ($R_{sh}$ = 8.6 Ohm/sq and $T$ = 74.4%). Layering the AgNW network between AZO films decreased the surface roughness ($R_{rms}$ < 8 nm) and enhances the mechanical flexibility of the hybrid films. The combination of these characteristics makes the hybrid film an excellent candidate for substrates of novel flexible optoelectronic devices which require high-temperature processing.

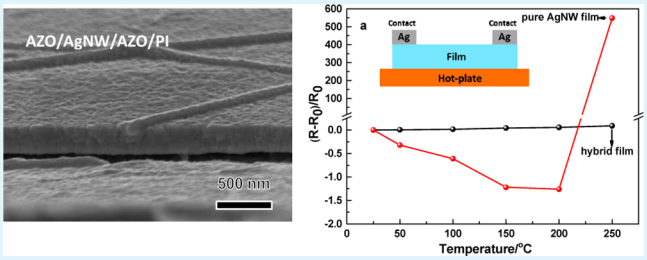


**KEYWORDS:** *transparent polyimide substrate, transparent conductive films, mechanical flexibility, thermal stability*

## 1. INTRODUCTION

Transparent conductive films (TCFs) are crucial components of optoelectronic devices, including flat panel displays, touch screens, light-emitting diodes, and solar cells.[1−8] Indium tin oxide (ITO) is a commonly used TCF material because of its advantageous trade-off between conductivity and transparency.[9,10] However, the use of ITO in large-area and low-cost devices is undesirable as it requires expensive vacuum deposition techniques; additionally, indium is a scarce material.[11]

Increasing efforts in developing nanomaterial TCFs have been observed recently, including silver nanowire (AgNW) films,[12] metal grids,[13,14] conjugated polymers,[15] carbon nanotubes,[16−18] and graphenes.[19,20] Of these examples, AgNW films show great promise as they display desirable electrical and optical properties. Furthermore, AgNW films can be deposited onto substrates using the solution deposition method, allowing for low-cost and high-throughput fabrication of devices.[21] Although promising, pure AgNW films suffer several drawbacks, including poor adhesion to substrate and large surface roughness.[22,23] Sandwich structures composed of an AgNW film and a metal−oxide layer have been suggested as promising alternatives to overcome these issues.[24−26]

Metal−oxide layers were introduced to improve the adhesion of the AgNW film to the substrate. Furthermore, this hybrid film facilitated effective charge carrier collection, both by filling the empty spaces between the AgNW/substrate interface and by smoothing the film surface. We recently reported an aluminum-doped zinc oxide (AZO)/AgNW/AZO hybrid film on a polyethylene terephthalate (PET) substrate which displayed a sheet resistance of 27.6 Ohm/sq and transmittance of 80.5%.[26] However, the hybrid films on PET substrates subjected to a lower glass transition temperature ($T_g$) of PET ($T_g$ = 62 °C for commonly used PET[27]) show a clear disadvantage, where their thermostability is poor and limits their applications.

A highly transparent polyimide (PI) substrate which was ∼50 μm thick with an optical transmittance of 90.2% at 550 nm was prepared on a glass plate. AZO/AgNW/AZO hybrid films were then successfully fabricated by combining sputtering and rod-coating processes on the transparent PI substrate. The hybrid film exhibited a low sheet resistance of 8.6 Ohm/sq and a high transmittance of 74.4%. Importantly, they also showed excellent thermal stability, mechanical flexibility, and adhesion.

## 2. EXPERIMENTAL PROCEDURES

**2.1. Materials.** The reagents used in this study included silver nitrate ($AgNO_3$), poly(vinylpyrrolidone) (PVP, K-30), sodium chloride (NaCl), ethylene glycol (EG), acetone, ethanol, and *N*,*N*-dimethylacetamide (DMAc). All reagents were of analytical grade and purchased from Sinopharm Chemical Reagent Co., Ltd. All chemicals were used as received without further purification.

**2.2. Synthesis of Silver Nanowires.** Silver nanowires were fabricated using a modified polyol reduction. Approximately 0.5 g of PVP was dissolved in 50 mL of EG by heating the solution to 170 °C with stirring for 1 h. A NaCl solution (50 μL 0.1 M in EG) was then added into the flask and stirred for 10 min. A $AgNO_3$ solution (50 mL,

Received: December 10, 2014
Accepted: January 28, 2015
Published: January 28, 2015

  

DOI: 10.1021/am508704u
ACS Appl. Mater. Interfaces 2015, 7, 4299−4305

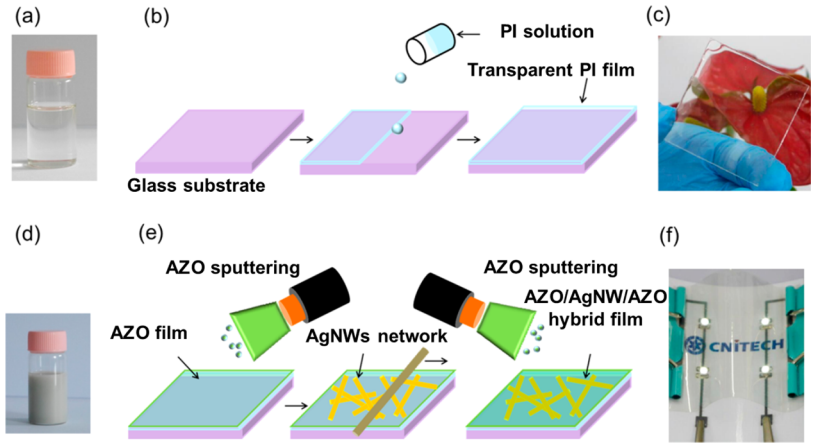


**Figure 1.** (a) Optical image of the PI solution, (b) schematic of the preparation for the transparent PI substrate, (c) highly transparent PI substrate on a glass plate, (d) optical image of AgNW dispersion, (e) schematic of the fabrication of AZO/AgNW/AZO/PI hybrid films, and (f) working LED circuits connected by highly transparent and flexible AZO/AgNW/AZO hybrid films.

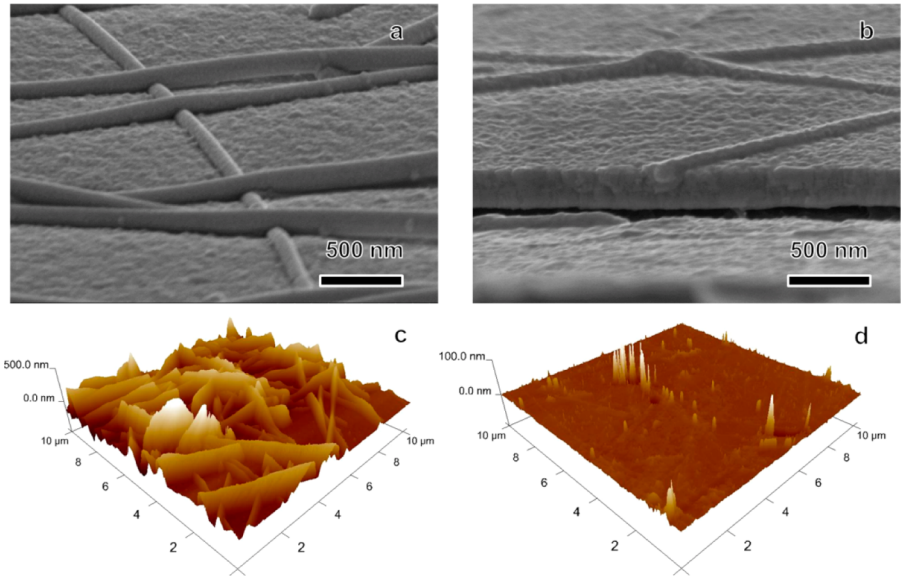


**Figure 2.** Cross-sectional images of the (a) AgNW/AZO and (b) AZO/AgNW/AZO hybrid films. Surface roughness of the (c) AgNW/AZO and (d) AZO/AgNW/AZO hybrid films.

0.059 M in EG) was subsequently added to the flask dropwise at a rate of 5 mL/min. The clear solution changed colors through yellow, red-orange, green, dark gray, and finally to glistening gray, which indicated the formation of long AgNWs. The reaction was allowed to cool to ambient temperature after 20 min. The solution was then centrifuged (3 times at 2000 rpm) to remove EG, PVP, and other impurities from the supernatant after adding acetone. The AgNWs were suspended in ethanol at a concentration of 0.2 mg·mL$^{-1}$ (Figure 1d). The length and diameter of the AgNWs was ∼12 $\mu$m and ∼75 nm, respectively.

**2.3. Synthesis of the Transparent PI Substrate.** The PI powder used to prepare the highly transparent PI films was synthesized according to our previous studies.[28] A clear PI solution in DMAc (10 wt %) was prepared (Figure 1a). The preparation of the transparent PI film, which typically resulted in a ∼50 $\mu$m thick layer, is illustrated schematically in Figure 1b. After the PI solution was cast on a clean glass plate, it was heated in an oven at 80 °C for 2 h to remove the solvent and then subjected to a heating schedule of 100, 150, and 200 °C for 60 min at each temperature. The transparent PI substrate displayed an optical transmittance of 90.2% at 550 nm (Figure 1c).

**2.4. Fabrication of the AZO/AgNW/AZO/PI Hybrid Film.** AZO/AgNW/AZO hybrid films were deposited on top of the transparent PI substrate using the RF sputtering and rod-coating method. Both top and bottom AZO layers were sputtered using an AZO target at 200 °C with a contrast RF power of 200 W, an Ar flow of 30 sccm, and a working pressure of 3 mTorr. The AgNW layer was deposited on the bottom AZO layer with $N$ numbers of rod-coating cycles and then dried at 60 °C for 3 min to remove the solvent before the top AZO layer was deposited. A schematic of the process is shown in Figure 1e.

To test the effectiveness of the transparent and flexible hybrid films, a simple conductive circuit was fabricated by depositing silver nanoparticle ink on a photo paper substrate. This was done using inkjet printing methods according to published procedures.[26] Both the AZO/AgNW/AZO hybrid film and LEDs were incorporated into the circuit. The hybrid film was tested after 500 inner bending cycles and successfully powered the LEDs which were visible through the transparent hybrid film (Figure 1f).

Furthermore, the pure AZO films and pure AgNW films were also prepared by depositing under the same conditions without the AgNW layer and by the rod coating of the AgNW suspension, respectively.

**2.5. Characterization.** Surface and cross-section morphologies of the AgNW/AZO and AZO/AgNW/AZO hybrid films were examined using scanning electron microscopy (SEM, Hitachi S-4800). The surface roughness of the AgNW/AZO and AZO/AgNW/AZO hybrid


DOI: 10.1021/am508704u
ACS Appl. Mater. Interfaces 2015, 7, 4299−4305

films was examined using an atomic force microscope (AFM, Veeco Dimension3100V). The silver content of the AZO/AgNW/AZO hybrid films was quantified using inductively coupled plasma optical emission spectroscopy (Agilent 700 Series). AZO/AgNW/AZO hybrid films were submersed in 65% nitric acid solutions for 30 min to completely dissolve the AgNWs. The solutions were then transferred to volumetric flasks. The optical transmittance of the pure AZO and AZO/AgNW/AZO hybrid films was determined at room temperature using a UV−vis spectrophotometer (PerkinElmer, Lambda 950, USA) with an integrating sphere. The sheet resistance was measured using a four-point probe system (Cresbox, Napson Corp.). The mechanical stability test was performed using a lab-made bending test machine. The adhesion test was performed using 3M stock tapes. The thermal stability test was performed by measuring the variation in the film resistance as a function of temperature.

## 3. RESULTS AND DISCUSSION

**3.1. Microstructure of AZO/AgNW/AZO Hybrid Films.** A cross-sectional image of a AgNW/AZO/PI hybrid film after sintering at 200 °C for 10 min is shown in Figure 2a. The sintered AgNWs were packed densely, forming a well-contacted network. When the top AZO film was sputtered at 200 °C, the final thickness of the AZO/AgNW/AZO/PI hybrid film was ~200 nm (Figure 2b). The individual AgNWs were naturally interconnected at their junctions during the AZO deposition. The toughing point of the AgNW network eats each other and forms a firm thermowelding junction that conducts after the thermal annealing process. The mean surface roughness of the AgNW/AZO/PI film was 93.7 nm (Figure 2c), which was significantly larger than that of the final AZO/AgNW/AZO/PI hybrid film (7.28 nm, Figure 2d). Thus, the top AZO layer both protected the AgNW network from oxidation and decreased the surface roughness of the AgNW network by filling the area between AgNWs.[29]

SEM images of AZO/AgNW/AZO/PI hybrid films with different numbers of AgNW rod-coating cycles ($N$) are shown in Figure 3. The density of the AgNW network increased as $N$ increased, as can be seen in Figure 3a−d. The AgNWs exhibited well-connected wire−wire junctions, and AgNWs embedded into the AZO films showed a randomly percolated network structure. The corresponding mass density of the AgNWs in the hybrid films increased from 5.8 to 40.3 mg/m$^2$ with the increasing numbers of $N$.

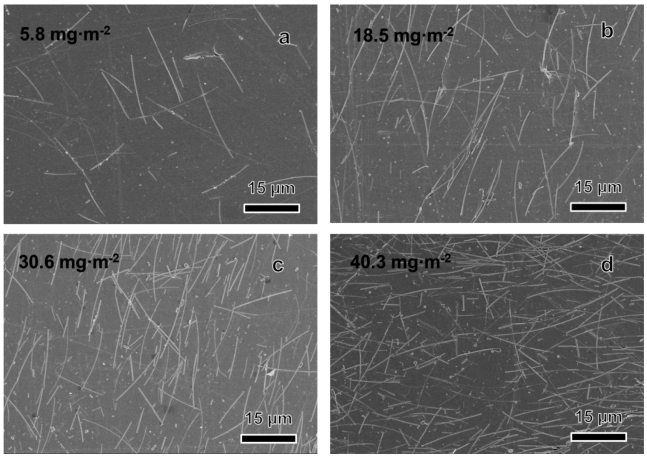


**Figure 3.** SEM images and corresponding mass density of the AgNW of the AZO/AgNW/AZO/PI hybrid films with different numbers of rod-coating cycles: (a) $N$ = 1, (b) $N$ = 3, (c) $N$ = 5, (d) $N$ = 8.

**3.2. Electrical and Optical Properties of AZO/AgNW/AZO/PI Hybrid Films.** The optical transmittance spectra of the hybrid films with increasing numbers $N$ are shown in Figure 4; the sheet resistance values of each film are also given. The pure AZO film displayed a high optical transmittance of 87.9% at 550 nm with a sheet resistance of 80.3 Ohm/sq. The hybrid film transmittance decreased as the number of $N$ increased. This change was caused by light reflection and scattering from both the AgNWs and the AgNW/AZO interface.

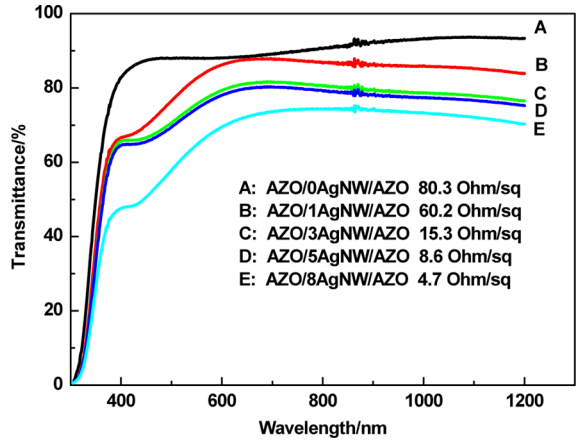


**Figure 4.** Optical transmittance and sheet resistance of the AZO/AgNW/AZO hybrid films.

The sheet resistance of the hybrid films decreased as $N$ increased. The AZO/1AgNW/AZO ($N$ = 1) sample displayed a sheet resistance of 60.2 Ohm/sq with a transmittance of 82.6% at 550 nm, whereas the AZO/8AgNW/AZO ($N$ = 8) sample displayed a sheet resistance of 4.7 Ohm/sq with a transmittance of 64.7% at 550 nm. These results indicated that the AgNW density can be adjusted to optimize the optical and electrical properties of AZO/AgNW/AZO hybrid films. The sheet resistance and optical transmittance at 550 nm were used to determine which hybrid film displayed the best electro-optical performance by calculating the figure of merit ($\Phi$) as defined by the Haacke equation[30]

$$\phi = \frac{T^{10}}{R_s} \quad (1)$$

where $T$ and $R_s$ are the transmittance at 550 nm and sheet resistance of the hybrid films, respectively. The hybrid film with optimal optoelectronic characteristics was the AZO/5AgNW/AZO ($N$ = 5) sample which had a $\Phi$ value of 6.0 × 10$^{-3}$ Ω$^{-1}$ (Table 1), which is larger than our previously reported record of 4.1 × 10$^{-3}$ Ω$^{-1}$ when deposited on a PET substrate.[25] The following equation was used to elucidate the electrical

**Table 1. Comparison of the Electrical and Optical Properties of the Pure AZO Film and AZO/AgNW/AZO Hybrid Films**

| rod-coating cycles ($N$) | $T_{550\ nm}$ (%) | $R_s$ (Ohm/sq) | figure of merit ($10^{-3}$ Ω$^{-1}$) |
|---|---|---|---|
| 0 | 87.9 | 80.3 | 3.4 |
| 1 | 82.6 | 60.2 | 2.5 |
| 3 | 75.6 | 15.3 | 4.0 |
| 5 | 74.4 | 8.6 | 6.0 |
| 8 | 64.7 | 4.7 | 2.7 |


DOI: 10.1021/am508704u
ACS Appl. Mater. Interfaces 2015, 7, 4299−4305

contribution of the AgNWs in AZO/AgNW/AZO hybrid films[31]

$$\frac{1}{R_{total}} = \frac{2}{R_{AZO}} + \frac{1}{R_{AgNW}} \quad (2)$$

where $R_{total}$, $R_{AZO}$, and $R_{AgNW}$ are the sheet resistance of the hybrid, AZO, and AgNW films, respectively. The AZO layers were sputtered on the PI substrate at 200 °C, which can decrease the sheet resistance of the AZO layers. We reported that the sheet resistance of a pure AZO layer (80.3 Ohm/sq) is lower than that of AZO sputtered at room temperature onto a PET substrate (308.7 Ohm/sq).[26] Furthermore, the use of higher sputtering temperature promoted fusing of the AgNW network, which also resulted in lower sheet resistance value. This "synergistic effect" helped to improve the Φ values of the AZO/AgNW/AZO/PI hybrid films.

**3.3. Mechanical Properties of AZO/AgNW/AZO/PI Hybrid Films.** Both outer bending and inner bending tests were performed using a lab-made apparatus at a fixed bending radius of 3 mm (Figure 5a and 5b). The tests involved different numbers of bending cycles. The mechanical flexibility of a pure AZO and AZO/AgNW/AZO hybrid films was compared. The nominal bending strain can be calculated using the following equation[32]

$$\varepsilon_f = \frac{h}{2r} \quad (3)$$

where $\varepsilon_f$, $h$, and $r$ are the nominal bending strain, substrate thickness, and bending radius, respectively. The typical bending strain in our study was 0.83%.

The surface morphologies of the pure AZO and AZO/5AgNW/AZO ($N$ = 5) hybrid films after 500 cycles of the outer bending test are shown in Figure 5c and 5d, respectively. Cracks are visible in both films. Near straight-line cracks, perpendicular to the tension direction, were observed when the bending cycles reached a critical value. The spacing of the cracks in the pure AZO film was closer than that of the hybrid film, which led to a sharp increase in the electrical resistance. Notably, the embedded AgNW layer in the AZO/5AgNW/AZO ($N$ = 5) hybrid film acted as a conducting bridge to connect the broken AZO film and hinder crack propagation after 500 cycles of the outer bending test. This phenomenon is attributed to the flexible and ductile nature of the AgNWs, which in turn enhanced the flexibility of the hybrid films.

The surface morphologies of the pure AZO film after 300 cycles and the AZO/5AgNW/AZO ($N$ = 5) hybrid films after 500 cycles of the inner bending test are shown in Figure 5e and 5f, respectively. As the defect density between the AZO film and the AgNW network was relatively large, cracks in the hybrid film were not straight but polyline under compression. The cracks propagated preferentially along the AZO/AgNW interfaces while breaking the wires when the crack initiated in AZO encountered the AgNWs.[33] Thus, delamination occurred during the inner bending test, which was more destructive to the hybrid films than that of the outer bending test.

The change in the sheet resistance as a function of bending cycles for the pure AZO and AZO/AgNW/AZO hybrid films is shown in Figure 6. The change in the film resistance ($R_c$) can be expressed as

$$R_c = (R - R_0)/R_0 \quad (4)$$

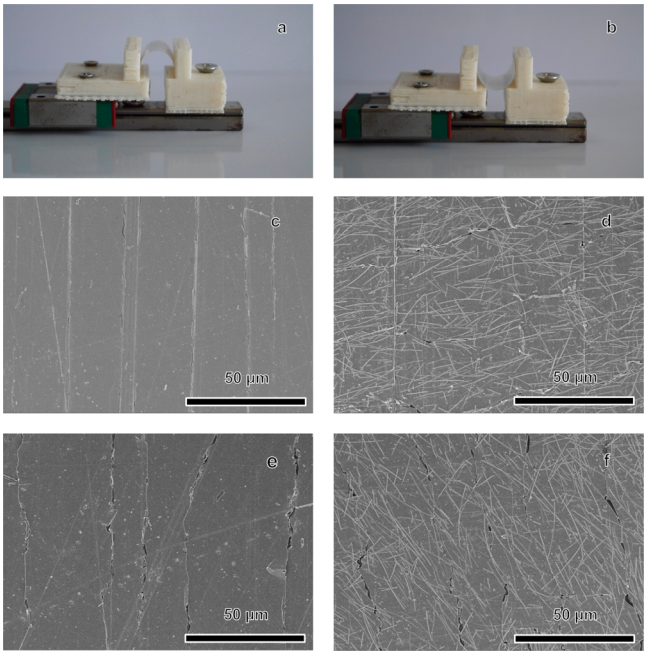


**Figure 5.** Photograph of the laboratory-made (a) outer and (b) inner bending test machine used in this study. Surface morphologies of the (c) pure AZO and (d) AZO/5AgNW/AZO hybrid films after 500 cycles of outer bending test. Surface morphologies of the (e) pure AZO film and (f) AZO/5AgNW/AZO hybrid films after 300 and 500 cycles of inner bending test, respectively.

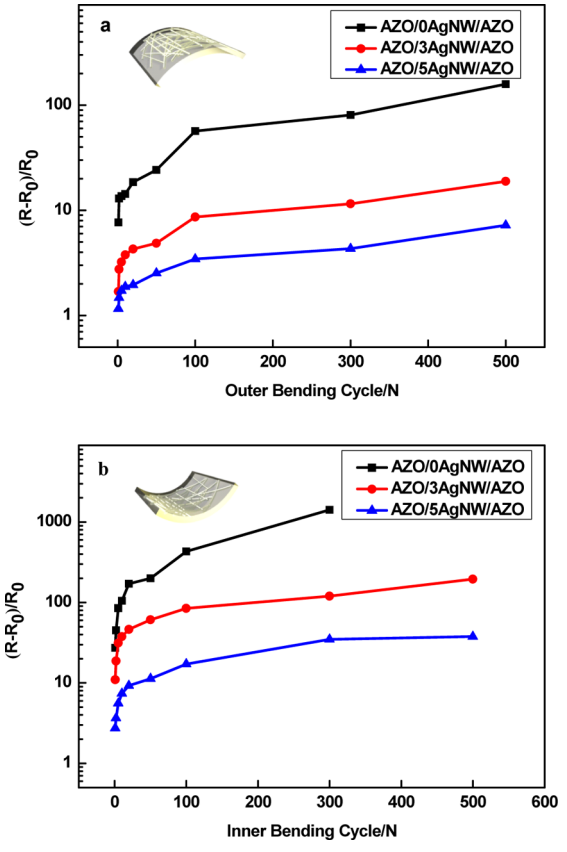


**Figure 6.** Sheet resistance change in the pure AZO and AZO/AgNW/AZO hybrid films: (a) outer bending test and (b) inner bending test.



DOI: 10.1021/am508704u
ACS Appl. Mater. Interfaces 2015, 7, 4299−4305

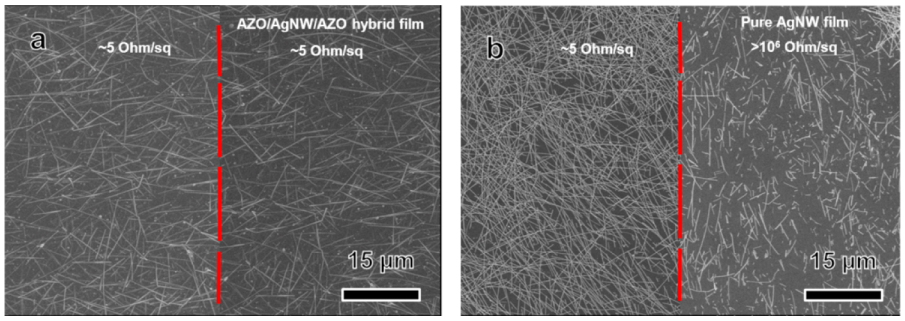


**Figure 7.** SEM images of the (a) AZO/AgNW/AZO hybrid and (b) pure AgNW films before (left) and after (right) the 3M taping test.

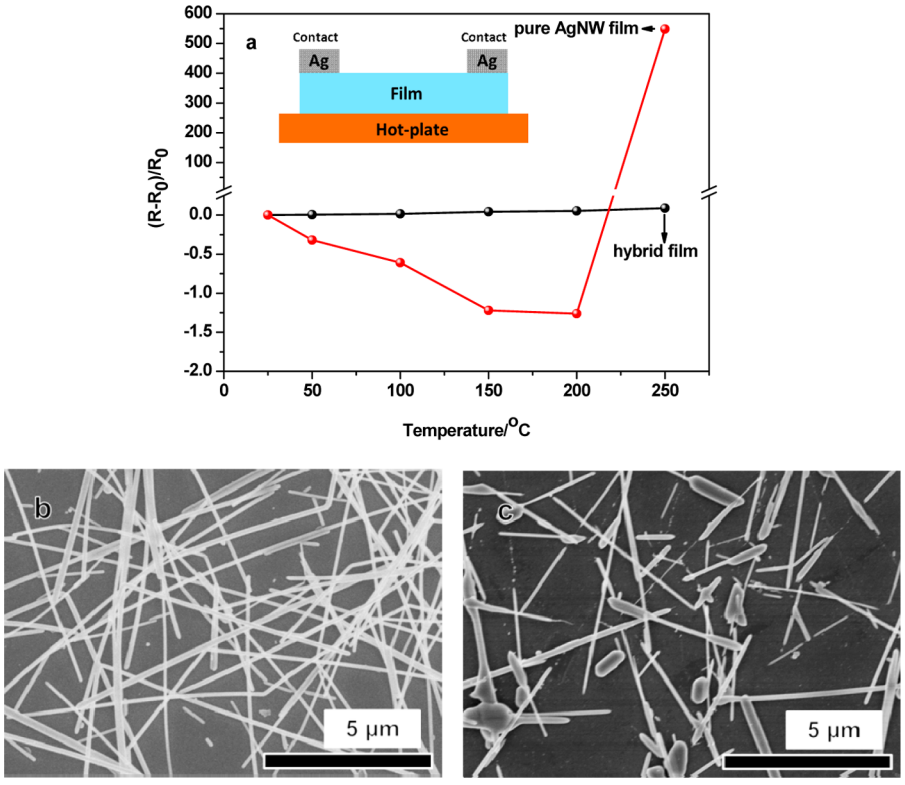


**Figure 8.** (a) Thermal stability of the AZO/AgNW/AZO hybrid and pure AgNW films with different annealing temperatures. Surface morphologies of the (b) AZO/AgNW/AZO hybrid and (c) pure AgNW films after annealed at 250 °C for 1 h.

where $R_0$ is the initial sheet resistance and $R$ is the value as measured after the bending test. Resistance changes were recorded three times for each bending cycle. AZO films are fragile and inflexible. The pure AZO film cracked in the initial stages of the outer bending test. After the cracks has formed, the film displayed a sharp increase in sheet resistance.[34] The sheet resistance changes in both the pure AZO and the AZO/AgNW/AZO hybrid films after the outer bending test are shown in Figure 6a. The AZO film exhibited a large increase in resistance due to crack formation and propagation with increasing numbers of bending cycles.[35] The value of $R_c$ for the pure AZO film after 500 outer bending cycles was 158. In contrast, the value of $R_c$ for the AZO/5AgNW/AZO ($N$ = 5) hybrid film after 500 bending cycles was 7. The considerable reduction in the value of $R_c$ for the hybrid film was attributed to the flexibility imparted by the AgNWs embedded between the inorganic metal oxide films. The sheet resistance changes in the pure AZO and AZO/AgNW/AZO hybrid films after the inner bending test are shown in Figure 6b. As expected, a large $R_c$ value of 1420 was observed for the pure AZO film after only 300 inner bending cycles. The electrical conductance of pure AZO was severely damaged. However, the AZO/5AgNW/AZO ($N$ = 5) hybrid film exhibited a $R_c$ value of less than 40, even after 500 bending cycles. Notably, the values of $R_c$ for the inner bending test were greater than those of the outer bending test. These results were attributed to different fracture mechanisms between the two tests. Additionally, the delamination that occurred in the inner bending test was more destructive than the cracking.

Adhesion is critical for successful flexible devices. To test the adhesion of the hybrid films to the substrates, 3M tape was applied to the films and then peeled off. SEM images of an AZO/AgNW/AZO hybrid film and a pure AgNW film before and after the adhesion test are shown in Figure 7. The AZO/AgNW/AZO hybrid film did not show any visible film destruction (Figure 7a), and the corresponding sheet resistance values remained consistent (~5 Ohm/sq). Conversely, the adhesion of the pure AgNW film to the substrate was poor


DOI: 10.1021/am508704u
ACS Appl. Mater. Interfaces 2015, 7, 4299−4305

(Figure 7b). The sheet resistance of the pure AgNW film increased from 5.0 to >$10^6$ Ohm/sq after the 3M taping test. These results suggested that the hybrid films had a strong mechanical adhesion to the substrate because the AgNWs were covered by the top AZO layer and embedded into both AZO layers, which prevented film detachment.

**3.4. Thermal Stability of AZO/AgNW/AZO/PI Hybrid Films.** The thermal stability of the pure AgNW and AZO/AgNW/AZO hybrid films on PI substrates was examined by heating the films and testing the change in resistance. A plot of the change in resistance as a function of temperature is shown in Figure 8a. A gradual decrease in sheet resistance of the pure AgNW film was observed up to 200 °C. This indicated the contacts between the AgNWs were fusing together. However, a clear rise in sheet resistance was observed when the film was annealed in air at 250 °C for 1 h (Figure 8c). This result was attributed to heat-induced welding of adjacent AgNWs, and the AgNW network was due to partial coalescence.[36] The morphology of the AZO/AgNW/AZO hybrid films remained intact without any melt down or disconnections after annealing in air at 250 °C for 1 h (Figure 8b). This result indicated that the hybrid film had greater thermostability than the pure AgNW film. The high-temperature stability of the hybrid film resulted from the AgNW film being effectively protected by the thermally stable AZO films.

## 4. CONCLUSIONS

A highly transparent PI substrate with an optical transmittance of 90.2% at 550 nm was synthesized by simple casting of the PI solution onto a glass plate. AZO/AgNW/AZO hybrid films were fabricated by combining sputtering and rod-coating processes on top of the transparent PI substrate. By adjusting the number of AgNW rod-coating cycles, a typical hybrid film with a low sheet resistance of 8.6 Ohm/sq, a high transmittance of 74.4%, and a figure of merit of $6.0 \times 10^{-3}$ $\Omega^{-1}$ was obtained. The mechanical properties of pure AZO and AZO/AgNW/AZO hybrid films were also investigated. The hybrid film displayed superior outer bending flexibility over inner bending. The higher $T_g$ value of the PI substrate enable annealing of the hybrid films at temperatures up to 250 °C for 1 h, at which the films remained stable. The reported TCFs containing AZO/AgNW/AZO/PI hybrid films displayed high transparency, excellent conductivity, flexibility, and thermal stability. As such, they have significant potential for applications in high-performance, flexible electronics, energy storage, and photovoltaic devices.

## AUTHOR INFORMATION

### Corresponding Authors

*E-mail: wfshen@nimte.ac.cn.
*E-mail: weijiesong@nimte.ac.cn.

### Notes

The authors declare no competing financial interest.

## ACKNOWLEDGMENTS

This work has been supported by the National Natural Science Foundation of China (Grant Nos. 21205127, 51403225, 21203226, 21377063).

## REFERENCES

(1) Eom, S. H.; Senthilarasu, S.; Uthirakumar, P.; Yoon, S. C.; Lim, J.; Lee, C.; Lim, H. S.; Lee, J.; Lee, S.-H. Polymer Solar Cells Based on Inkjet-Printed PEDOT:PSS Layer. *Org. Electron.* **2009**, *10*, 536−542.
(2) Ellmer, K. Past Achievements and Future Challenges in the Development of Optically Transparent Electrodes. *Nat. Photonics* **2012**, *6*, 809−817.
(3) Mirri, F.; Ma, A. W. K.; Hsu, T. T.; Behabtu, N.; Eichmann, S. L.; Young, C. C.; Tsentalovich, D. E.; Pasquali, M. High-Performance Carbon Nanotube Transparent Conductive Films by Scalable Dip Coating. *ACS Nano* **2012**, *6*, 9737−9744.
(4) Zhao, Y.; Zhang, Y.; Li, Y.; He, Z.; Yan, Z. Rapid and Large-Scale Synthesis of Cu Nanowires Via a Continuous Flow Solvothermal Process and Its Application in Dye-Sensitized Solar Cells (Dsscs). *RSC Adv.* **2012**, *2*, 11544−11551.
(5) Kamyshny, A.; Magdassi, S. Conductive Nanomaterials for Printed Electronics. *Small* **2014**, *10*, 3515−3535.
(6) Song, J.; Li, J.; Xu, J.; Zeng, H. Super-Stable Transparent Conductive Cu@ $Cu_4Ni$ Nanowire Elastomer Composites against Oxidation, Bending, Stretching and Twisting for Flexible and Stretchable Optoelectronics. *Nano Lett.* **2014**, *14*, 6298−6305.
(7) Makino, H.; Song, H.; Yamamoto, T. Influences of Oxygen Gas Flow Rate on Electrical Properties of Ga-Doped ZnO Thin Films Deposited on Glass and Sapphire Substrates. *Thin Solid Films* **2014**, *559*, 78−82.
(8) Song, J.; Kulinich, S. A.; Li, J.; Liu, Y.; Zeng, H. A General One-Pot Strategy for the Synthesis of High-Performance Transparent-Conducting-Oxide Nanocrystal Inks for All-Solution-Processed Devices. *Angew. Chem., Int. Ed.* **2014**, *54*, 462−466.
(9) Ghosh, D.; Martinez, L.; Giurgola, S.; Vergani, P.; Pruneri, V. Widely Transparent Electrodes Based on Ultrathin Metals. *Opt. Lett.* **2009**, *34*, 325−327.
(10) Hecht, D. S.; Hu, L.; Irvin, G. Emerging Transparent Electrodes Based on Thin Films of Carbon Nanotubes, Graphene, and Metallic Nanostructures. *Adv. Mater.* **2011**, *23*, 1482−1513.
(11) Kim, A.; Won, Y.; Woo, K.; Jeong, S.; Moon, J. All-Solution-Processed Indium-Free Transparent Composite Electrodes Based on Ag Nanowire and Metal Oxide for Thin- Film Solar Cells. *Adv. Funct. Mater.* **2014**, *24*, 2462−2471.
(12) Langley, D.; Giusti, G.; Mayousse, C.; Celle, C.; Bellet, D.; Simonato, J. P. Flexible Transparent Conductive Materials Based on Silver Nanowire Networks: A Review. *Nanotechnology* **2013**, *24*, 452001.
(13) Zou, J.; Yip, H.-L.; Hau, S. K.; Jen, A. K.-Y. Metal Grid/Conducting Polymer Hybrid Transparent Electrode for Inverted Polymer Solar Cells. *Appl. Phys. Lett.* **2010**, *96*, 203301.
(14) Han, B.; Pei, K.; Huang, Y.; Zhang, X.; Rong, Q.; Lin, Q.; Guo, Y.; Sun, T.; Guo, C.; Carnahan, D.; Giersig, M.; Wang, Y.; Gao, J.; Ren, Z.; Kempa, K. Uniform Self-Forming Metallic Network as a High-Performance Transparent Conductive Electrode. *Adv. Mater.* **2014**, *26*, 873−877.
(15) Xia, Y.; Sun, K.; Ouyang, J. Solution-Processed Metallic Conducting Polymer Films as Transparent Electrode of Optoelectronic Devices. *Adv. Mater.* **2012**, *24*, 2436−2440.
(16) Wu, Z.; Chen, Z.; Du, X.; Logan, J. M.; Sippel, J.; Nikolou, M.; Kamaras, K.; Reynolds, J. R.; Tanner, D. B.; Hebard, A. F. Transparent, Conductive Carbon Nanotube Films. *Science* **2004**, *305*, 1273−1276.
(17) De Volder, M. F.; Tawfick, S. H.; Baughman, R. H.; Hart, A. J. Carbon Nanotubes: Present and Future Commercial Applications. *Science* **2013**, *339*, 535−539.
(18) Park, S.; Vosguerichian, M.; Bao, Z. A Review of Fabrication and Applications of Carbon Nanotube Film-Based Flexible Electronics. *Nanoscale* **2013**, *5*, 1727−52.
(19) Wu, J.; Becerril, H. A.; Bao, Z.; Liu, Z.; Chen, Y.; Peumans, P. Organic Solar Cells with Solution-Processed Graphene Transparent Electrodes. *Appl. Phys. Lett.* **2008**, *92*, 263302.
(20) Rana, K.; Singh, J.; Ahn, J.-H. A Graphene-Based Transparent Electrode for Use in Flexible Optoelectronic Devices. *J. Mater. Chem. C* **2014**, *2*, 2646−2656.


DOI: 10.1021/am508704u
*ACS Appl. Mater. Interfaces* 2015, 7, 4299−4305

(21) De, S.; Higgins, T. M.; Lyons, P. E.; Doherty, E. M.; Nirmalraj, P. N.; Blau, W. J.; Boland, J. J.; Coleman, J. N. Silver Nanowire Networks as Flexible, Transparent, Conducting Films: Extremely High Dc to Optical Conductivity Ratios. *ACS Nano* **2009**, *3*, 1767−1774.
(22) Hu, L.; Kim, H. S.; Lee, J.-Y.; Peumans, P.; Cui, Y. Scalable Coating and Properties of Transparent, Flexible, Silver Nanowire Electrodes. *ACS Nano* **2010**, *4*, 2955−2963.
(23) Zeng, X. Y.; Zhang, Q. K.; Yu, R. M.; Lu, C. Z. A New Transparent Conductor: Silver Nanowire Film Buried at the Surface of a Transparent Polymer. *Adv. Mater.* **2010**, *22*, 4484−8.
(24) Choi, K.-H.; Kim, J.; Noh, Y.-J.; Na, S.-I.; Kim, H.-K. Ag Nanowire-Embedded ITO Films as a near-Infrared Transparent and Flexible Anode for Flexible Organic Solar Cells. *Sol. Energy Mater. Sol. Cells* **2013**, *110*, 147−153.
(25) Kim, A.; Won, Y.; Woo, K.; Kim, C.-H.; Moon, J. Highly Transparent Low Resistance ZnO/Ag Nanowire/ZnO Composite Electrode for Thin Film Solar Cells. *ACS Nano* **2013**, *7*, 1081−1091.
(26) Xu, Q.; Shen, W.; Huang, Q.; Yang, Y.; Tan, R.; Zhu, K.; Dai, N.; Song, W. Flexible Transparent Conductive Films on Pet Substrates with an AZO/AgNW/AZO Sandwich Structure. *J. Mater. Chem. C* **2014**, *2*, 3750−3755.
(27) Brandrup, J.; Immergut, E. H.; Grulke, E. A.; Abe, A.; Bloch, D. R. *Polymer Handbook*; Wiley: New York, 1999; Vol. *89*.
(28) Chen, G. F.; Pei, X. L.; Liu, J. T.; Fang, X. Z. Synthesis and Properties of Transparent Polyimides Derived from Trans- and Cis-1,4-Bis(3,4-Dicarboxyphenoxy) Cyclohexane Dianhydrides. *J. Polym. Res.* **2013**, *20*, 159.
(29) Lee, H. J.; Hwang, J. H.; Choi, K. B.; Jung, S. G.; Kim, K. N.; Shim, Y. S.; Park, C. H.; Park, Y. W.; Ju, B. K. Effective Indium-Doped Zinc Oxide Buffer Layer on Silver Nanowires for Electrically Highly Stable, Flexible, Transparent, and Conductive Composite Electrodes. *ACS Appl. Mater. Interfaces* **2013**, *5*, 10397−10403.
(30) Haacke, G. New Figure of Merit for Transparent Conductors. *J. Appl. Phys.* **1976**, *47*, 4086−4089.
(31) Choi, Y.-Y.; Choi, K.-H.; Lee, H.; Lee, H.; Kang, J.-W.; Kim, H.-K. Nano-Sized Ag-Inserted Amorphous Znsno3Multilayer Electrodes for Cost-Efficient Inverted Organic Solar Cells. *Sol. Energy Mater. Sol. Cells* **2011**, *95*, 1615−1623.
(32) Lewis, J. Material Challenge for Flexible Organic Devices. *Mater. Today* **2006**, *9*, 38−45.
(33) Cheong, H.-G.; Triambulo, R. E.; Lee, G.-H.; Yi, I.-S.; Park, J.-W. Silver Nanowire Network Transparent Electrodes with Highly Enhanced Flexibility by Welding for Application in Flexible Organic Light-Emitting Diodes. *ACS Appl. Mater. Interfaces* **2014**, *6*, 7846−7855.
(34) Choa, S.-H.; Cho, C.-K.; Hwang, W.-J.; Tae Eun, K.; Kim, H.-K. Mechanical Integrity of Flexible InZnO/Ag/InZnO Multilayer Electrodes Grown by Continuous Roll-to-Roll Sputtering. *Sol. Energy Mater. Sol. Cells* **2011**, *95*, 3442−3449.
(35) Ni, J. L.; Zhu, X. F.; Pei, Z. L.; Gong, J.; Sun, C.; Zhang, G. P. Comparative Investigation of Fracture Behaviour of Aluminium-Doped Zno Films on a Flexible Substrate. *J. Phys. D: Appl. Phys.* **2009**, *42*, 175404.
(36) Ghosh, D. S.; Chen, T. L.; Mkhitaryan, V.; Formica, N.; Pruneri, V. Solution Processed Metallic Nanowire Based Transparent Electrode Capped with a Multifunctional Layer. *Appl. Phys. Lett.* **2013**, *102*, 221111.


DOI: 10.1021/am508704u
*ACS Appl. Mater. Interfaces* 2015, 7, 4299−4305